Ultrasonics Sonochemistry 113 (2025) 107242

Contents lists available at ScienceDirect

Ultrasonics Sonochemistry

journal homepage: www.elsevier.com/locate/ultson

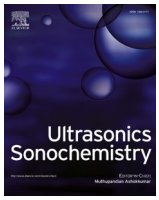

Functional nanocrystal as effective contrast agents for dual-mode imaging: Live-cell sonoluminescence and contrast-enhanced echography

V. Vighetto [a,b], E. Pascucci [a], N.M. Percivalle [a], A. Troia [c], K.M. Meiburger [b,d], M.R.P. van den Broek [e], T. Segers [e], V. Cauda [a,b,*]

[a] Department of Applied Science and Technology, Politecnico di Torino, Corso Duca degli Abruzzi 24, 10129 Turin, Italy
[b] Polito^{BIO}Med Lab, Politecnico di Torino, 10129 Turin, Italy
[c] Ultrasounds & Chemistry Lab, Advanced Metrology for Quality of Life, Istituto Nazionale di Ricerca Metrologica (I.N.Ri.M.), Strada delle Cacce 91, 10135 Turin, Italy
[d] Department of Electronics and Telecommunications, Politecnico di Torino, 10129 Turin, Italy
[e] BIOS/Lab on a Chip Group, Max-Planck Center Twente for Complex Fluid Dynamics, MESA+ Institute for Nanotechnology, University of Twente, Drienerlolaan 5, 7522 NB Enschede, Netherlands

ARTICLE INFO

Keywords:
Zinc oxide
Inertial cavitation
Sonoluminescence
Bubble cavitation
Echographic nano-contrast agent

ABSTRACT

In the context of molecular imaging, the present work explores an innovative platform made of lipid-coated nanocrystals as contrast-enhanced agent for both ultrasound imaging and sonoluminescence. At first, the dynamics of gas bubbles generation and cavitation under insonation with either pristine or lipid-coated nanocrystals (ZnO-Lip) are described, and the differences between the two colloidal systems are highlighted. These ZnO-Lip show an unprecedented ability to assist cavitation, which is reflected in enhanced sonoluminescent light emission with respect to the pristine nanocrystals or the pure water. Highly defined and sharp sonoluminescent images of cultured cells are indeed obtained, for the first time, when ZnO-Lip are used. Furthermore, ZnO-Lip were adopted as a nanosized agent for contrast-enhanced ultrasound imaging, i.e. echography, first in solutions, and then on ex-vivo tissues. A prolonged over time and bright imaging effect is observed when adopting the developed nanoparticles. Furthermore, their nanometric size and potential targeting with biomolecules would allow ease extravasation and tissue or even cell penetration, achieving enhanced-contrast imaging. Finally, the stimuli-responsive therapeutic applications of ZnO-Lip against tumors is overviewed, aiming to achieve a fully theranostic approach.

1. Introduction

Multimodal, molecular imaging allows the visualization of biological processes at cellular, subcellular and molecular-level resolutions using multiple, complementary imaging techniques[1]. Typically, molecular imaging involves the administration of an exogenous imaging agent in the form of a small molecule, macromolecule or nanoparticle (NP) to visualize, target and trace relevant physiological processes being studied. These imaging agents facilitate the real-time assessment of pathways and mechanisms *in vivo* and enhance both diagnostic and therapeutic efficacies[2,3].

The design of sophisticated contrast agents with high sensitivity and specificity towards the organ or tissue of interest is at the frontier of research[4–9]. It can provide a visual aid to assess not only the presence of a disease, e.g. cancer, but also the biodistribution and the biological effects of a therapeutic agent[10]. In this context, contrast agents were already introduced for diagnostic ultrasound imaging to guarantee stability and increase ultrasound scattering. The clinically-approved contrast agents are gas-filled microbubbles[11] having a size of several microns and application limited to the vascular compartment, since the extravasation is prevented by their size[10]. The key point to enable molecular imaging for ultrasound is thus the development of nano-sized contrast agents (i.e. smaller than 600 nm)[12,13] capable to extravasate, target cells or their components and generate sustained echogenic signals. Currently, various experimental approaches, as also pioneered by some of us[14], have attempted to stabilize gas nanobubbles on surfaces, developing a new class of nano-contrast agents. Various nanocrystals (NCs), including hydrophobic mesoporous silica,

* Corresponding author at: Department of Applied Science and Technology, Politecnico di Torino, Corso Duca degli Abruzzi 24, 10129 Turin, Italy Tel.: +39 011 090 7389.
E-mail address: valentina.cauda@polito.it (V. Cauda).

https://doi.org/10.1016/j.ultsonch.2025.107242
Received 3 December 2024; Received in revised form 9 January 2025; Accepted 20 January 2025
Available online 22 January 2025

solid polymeric (PTFE) NCs and amino-functionalized ZnO nanocrystals, able to immobilize surface nanobubbles were reported to act as cavitation nuclei under US stimulation and thereby provide contrast in ultrasound imaging.

Another imaging approach triggered by ultrasound waves and discovered almost 90 years ago is sonoluminescence (SL), i.e. the generation of UV–visible light from cavitation bubble collapse, which regained attention nearly 30 years ago after the discovery of single bubble SL [15]. However, these light emissions are particularly short-lasting (in the order of ps) and can be maintained over time under multibubble cavitation. SL has been already proposed in the biomedical field, as in the case of SL tomography[16], where the sonoluminescent light is produced in tissue during US irradiation. The differences in the attenuation of SL photons between various tissues, due to intrinsic anisotropy, scattering and absorption coefficients, create the needed contrast. SL as imaging method was also proposed to overcome the superficial depth of fluorescent molecular tomography. The idea was to excite dye molecules present in deep tissue through a small internal light source created during focused ultrasound irradiation of the area[17]. Recently, a similar approach was also demonstrated in vivo, exploiting ultrasound to activate luminescent molecules and NPs through two-step intraparticle energy conversion[18]. Indeed, in these few literature examples, an intermediate molecule with luminescence or fluorescent properties is present to convert SL emission into a brighter signal.

It is known that the cavitation threshold for activating SL in pure water require such high acoustic pressure, in terms of low frequencies and high-power US intensities, to become dangerous for living cells and tissues. Furthermore, the intensity of SL is per se very low and barely visible, requiring a specific set-up to allow detection or luminescent molecules able to amplify the produced light in a more powerful signal. It is generally recognized that the presence of micro or NPs (of whatever nature they are) in the liquid medium reduces the dose of US necessary to obtain acoustic inertial cavitation, because of their intrinsic ability to carry gas pockets on their structure due to their nanostructure, roughness or surface porosity, as we also recently proved[19]. To overcome the above-mentioned challenges in the SL bioimaging, we indeed reported that we can combine the SL emission in the acoustic field with a particular type of nanocrystals possessing well-defined optical properties, to obtain light emissions that can: i) amplify and ii) spectroscopically modify the initial SL emission[19]. This combination allowed a well-defined spectral emission signature, showing a peak intensity redistribution in the obtained SL spectrum due to the specific optical properties of the used NCs, in particular a semiconductor. While the previous work focused on water suspensions of ZnO nanocrystals, here we challenged the previous finding to propose an innovative bioimaging method based on NCs-assisted ultrasound for both SL and echographic imaging. In particular, the semiconductor and biodegradable ZnO NCs previously used, are here proposed as highly biocompatible iron-doped ZnO NCs wrapped in a biomimetic lipidic shell (ZnO-Lip). We show that our ZnO-Lip can increase and sustain in time the phenomenon of sonoluminescence in aqueous and biologically relevant media, investigating the dynamics of bubbles to which the signal is related. An in vitro image of cancerous cells, obtained acquiring sonoluminescent photons which are augmented by the presence of ZnO-Lip nanocrystals, is here produced and proposed for the first time at our knowledge. The same NCs are here verified to act also as an ultrasound contrast agent for sustained contrast-enhanced ultrasound imaging, enabling the dual use of this nanotool in the bioimaging field. These features enable a relatively simple imaging system, without introducing many different molecules or contrast agents, while simply relying on one type of highly biocompatible ZnO-Lip NCs.

As a final perspective, these NCs are shown as ultrasound responsive therapeutic agents too[20–23], adopting either acoustic shock waves of continuous planar US at specific frequencies and intensities. These multimodal interventions open a perspective in achieving an all-in-one platform for theranosic application, as specifically here reported against cancer diseases.

2. Materials and Methods

2.1. Nanocrystals synthesis and functionalization

Zinc oxide nanocrystals (ZnO) were synthesized by a wet chemical process, exploiting oleic acid (Sigma-Aldrich) as stabilizing agent, as reported elsewhere [24,25]. Concisely, zinc acetate dihydrate (526 mg, ACS Reagent, Sigma-Aldrich) was dissolved in 40 mL of ethanol and heated up to 70 °C. Bidistilled (b.d.) water (1 mL, from a Direct Q3 system, Millipore, Burlington) and oleic acid (140 μL) were added to the solution. Then, tetramethylammonium hydroxide (1.044 mg, TMAH, Sigma-Aldrich) earlier dissolved in bd water (1.052 mL) and ethanol (10 mL), was added to the zinc precursor solution to form the NCs. After 10 min, the NCs were collected and centrifuged at 10′000 g to be resuspended in fresh ethanol. Three washes with fresh ethanol were performed. ZnO surface was then functionalized with amino-propyl groups, adding 10 mol% of 3-aminopropyltrimethoxysilane (APTMS, Sigma-Aldrich) according to the literature [24–26]. More specifically, ZnO were dispersed in ethanol at a concentration of 2.5 mg/mL and heated up to 70 °C in nitrogen atmosphere and refluxing conditions. APTMS was added to the solution and the reaction was carried on for 6 h at 70 °C. At the end of the procedure, NCs were collected and washed three times by a centrifugation and redispersion process. ZnO NCs were stored as ethanol colloidal suspensions, according to previous works [24,27].

Z-Potential and Dynamic Light Scattering (DLS) measurements were performed with a Zetasizer Nano ZS90 (Malvern Instruments). The size of amino-propyl functionalized ZnO particles was measured in bd water at a concentration of 100 μg/mL. Z-Potential measurements were performed in b.d. water at a concentration of 100 μg/mL.

Functionalized ZnO nanocrystals were characterized with High Resolution Transmission Electron Microscopy (HR-TEM). NCs were dispersed in water at a concentration of 50 μg/mL. Then, 10 μL of the solution was deposited onto a Lacey Carbon Support Film (300 mesh, Cu, Ted Pella Inc.) and let to dry. The measurements were held with a Talos™ F200X G2 S(TEM) from Thermo Scientific at an operating voltage of 200 kV for ZnO while when the sample was ZnO-Lip the voltage was reduced to 60 kV and no staining was needed.

2.2. Lipid shell formation and nanocrystals encapsulation

The nanocrystals biocompatibility and colloidal stability were enhanced through the coating with a lipidic shell, which formulation was reported by some of us in a previous work [28]. Briefly, DOPA (1,2-dioleoyl-*sn*-glycero-3-phosphate dissolved in chloroform, by Avanti Polar Lipids), DOPC (1,2-dioleoyl-*sn*-glycero-3-phosphocholine dissolved in chloroform, by Avanti Polar Lipids), cholesterol (Sigma Aldrich) and DSPE-PEG(2000)-Amine (1,2-distearoyl-*sn*-glycero-3-phosphoethanolamine-n-[amino(polyethylene glycol)-2000] were mixed in a molar ratio of 50/10/38.5/1.5 and dried overnight under vacuum. Afterwards, the dried lipids were resuspended in a mixture of ethanol and water (with a volume ratio of 40/60), to obtain a 3 mg/mL lipidic solution. The lipidic solution was added to the pelleted ZnO NCs after centrifugation in a weight ratio of 2:1 and sonicated for 3 min at 59 kHz. Thereafter, a volume of bd water was added to allow the self-assembly of the lipidic shell on the surface of the nanocrystals and a final 1 mg/mL concentration of lipid-coated ZnO (ZnO-Lip) was achieved. A further sonication step for 5 min at 59 kHz was performed to increase homogeneity of the suspension.

2.3. Bubble cavitation measurements by ultra-high-speed imaging

Ultra-high-speed bright-field microscopy was employed to investigate the bubble dynamics aiming at the direct observation of ultrasound-driven bubble oscillations. To this end, a high-speed camera (HPV-X2,

Shimadzu) was mounted on a modular upright microscope (BX-FM, Olympus) equipped with a water dipping 40x objective (LUM-PlanFL, Olympus) and an additional 2x magnifying module resulting in an imaging resolution of 267 nm per pixel. Either ZnO or ZnO-Lip NCs were loaded in a custom-made 3D printed sample holder comprising two acoustically transparent 50-μm thick Melinex (duPont Teijin Films, Chester, Va) membranes spaced by 100 μm. The sample holder was placed in a water bath in the optical focus of the microscope. A focused ultrasound transducer (1 MHz center frequency, Evident, V314) was placed in the water bath as well, with its focus co-aligned with the optical focus. The sensitivity of the transducer was calibrated using a calibrated needle hydrophone (Precision Acoustics). The acoustic transmit pulses were 10 cycles in length, Gaussian tapered over the first and final 2 cycles, and they had a peak-negative acoustic pressure amplitude of 3.6 MPa. The transmit pulses were generated by an arbitrary waveform generator (Tabor, WW1074) connected to an amplifier (Vectawave, VBA100- 200). The illumination of the camera was provided by a high-intensity strobe light (MVS7010, Perkin-Elmer) connected to an optical fiber that was mounted below the NCs sample holder in the water bath. The high-speed camera, waveform generator, and strobe light were triggered using a pulse-delay generator (BNC 575, Berkeley Nucleonics).

2.4. Bubble characterization using acoustic attenuation measurements

Acoustic attenuation measurements were performed in a water tank in which two confocally aligned ultrasound transducers were mounted. The transmit transducer (2.25 MHz, Evident, V314) was used to transmit narrowband 10-cycle ultrasound pulses at frequencies ranging from 0.5 MHz up to 5 MHz in steps of 50 kHz at an acoustic pressure amplitude of 95 kPa. The acoustic pressure was kept constant across the employed frequency range by correcting the transmit voltage for the frequency dependent sensitivity of the transducer, which was measured using a calibrated hydrophone (Precision Acoustics). The transmission of each 10-cycle ultrasound pulse through a continuously steered suspension of either ZnO or ZnO-Lip NCs was measured using the receive transducer. The attenuation coefficient at each transmit frequency f_T was then calculated from a measurement with bubbles present, and from that of a reference measurement without bubbles present, as follows:

$$\alpha_{exp} = -\frac{10}{d}\log_{10}\frac{|V_{bub}(f_T)|^2}{|V_{ref}(f_T)|^2}.$$

Here, $|V_{bub}(f_T)|^2$ and $|V_{ref}(f_T)|^2$ are the amplitudes of the power spectra computed from the voltage–time signals with and without bubbles present at transmit frequency f_T, respectively, and d is the acoustic path length of 1 cm over which the NCs were present in the ultrasound field.

2.5. Sonoluminescence measurements

The proposed imaging system was designed with the aim of acquiring reliable data concerning the total emission generated by sonoluminescence in various solutions. Within this setup, the emitted light is captured using a CCD camera (Princeton Instruments) configured for full-chip operation (1340x100 pixels), thus ensuring the production of an output image. To mitigate the intrinsic thermal noise of the instrument, the camera is maintained at a temperature of −90 °C through liquid nitrogen cooling. The dish was subjected to ultrasound (US) using a biomedical device (Chattanooga, Intelect Mobile 2 COMBO from DJO France, ENOVIS) and the image was captured by the cooled CCD through a lens (4X) mounted on an inverted microscope (Nikon Eclipse Ti) directly connected to the CCD. Data acquisition was performed using WinSpec software (Princeton Instruments), see scheme in Fig. S1 of the Supporting Information S.I.

The exposure time was set to 120 s and 10 mL of solution was placed within each dish. Each solution underwent ultrasound treatment at a power density of 2 W/cm^2, DC 100 % at 1 MHz. Samples containing distilled water and samples containing complete cell culture medium (RPMI-1640 with 10 % fetal bovine serum, ATCC) were tested. Each solution was tested both in the absence and presence of ZnO and ZnO-Lip at two different concentrations (100 μg/mL and 200 μg/mL), to probe their ability as nano-contrast imaging agents.

The acquired data were subsequently processed using MATLAB. Once the data were loaded to the software, to compare the various solution combinations, the image corresponding to ultrasound treatment without ZnO and ZnO-Lip was subtracted from each image.

2.6. Cell culture

HT-29 cell line was cultured in RPMI (ATCC), supplemented with 10 % heat-inactivated fetal bovine serum (FBS, ATCC), 100 μg/mL streptomycin and 100 units/mL penicillin (Sigma), and 1 % l-glutamine (Sigma). Cells were maintained at 37 °C under a 5 % CO_2 atmosphere.

2.7. Sonoluminescence in in-vitro cell cultures and viability

10^5 HT-29 cells were seeded into each Petri dish with a diameter of 6 cm the day before the experiment to allow them time to adhere to the dish. The experimental setup was carried out similarly to what was described in paragraph 2.6 with the difference that, to maintain sterile cell culture outside the hood, the Petri dishes were sealed with a 0.18 mm Polyethylene terephthalate (PET) cap and wrapped with parafilm. Additionally, cell medium (RPMI-1640 with 10 % fetal bovine serum) was injected into the Petri dish using a syringe until completely filled, in order to eliminate air within the system and enable ultrasound propagation in the underlying liquid volume.

Two conditions were examined: one without the presence of ZnO-Lip in the medium and another with ZnO-Lip at a concentration of 100 μg/mL. For each condition, three images were acquired: one utilizing ambient light, subsequently referred to as “ambient white light” with an exposure of 300 ms; a second image was acquired for 120 s in the dark, used as a background to post-acquisition removal of both instrumental and ambient noise; finally, a third image was acquired in the dark for 120 s, during which ultrasound stimulation was applied with the same power density, frequency, and DC characteristics described in paragraph 2.5.

After acquiring the images for both conditions, they were processed using MATLAB software. Specifically, a pixel-by-pixel subtraction was performed between the image obtained in the dark with ultrasound stimulation and the image obtained in the dark without ultrasound stimulation. Pixels with excessively high and low intensities, considered spikes, were subsequently removed, and the mean intensity of all pixels in the final image was assigned to them. Finally, the resulting image was compared with the image obtained under ambient white light condition. Fig. 1 schematically illustrates the entire process of SL image acquisition and elaboration.

A cell viability test was conducted to assess the potential toxic effects of the imaging treatment described above on HT-29 cells. Four experimental conditions were tested in triplicate (n = 3): a control, a condition where cells received only ZnO-Lip at a concentration of 100 μg/mL, a condition where cells received only ultrasound stimulation, and finally a condition where both ZnO-Lip and ultrasound stimulation were present simultaneously at the imaging conditions. After performing ultrasound stimulation in the required conditions, cells for each condition were transferred to a 96-well plate at a concentration of 5000 cells per well. Additionally, wells containing only ZnO-Lip dispersed in RPMI were prepared. After 24 h of incubation, the WST-1 proliferation test (Roche, Basel, Switzerland) was performed. In summary, 10 μL of WST-1 reagent were added to the wells two hours before each reading and incubated at 37 °C in a 5 % CO_2 atmosphere. After two hours, absorbance was measured using a Multiskan GO microplate spectrophotometer (Thermo

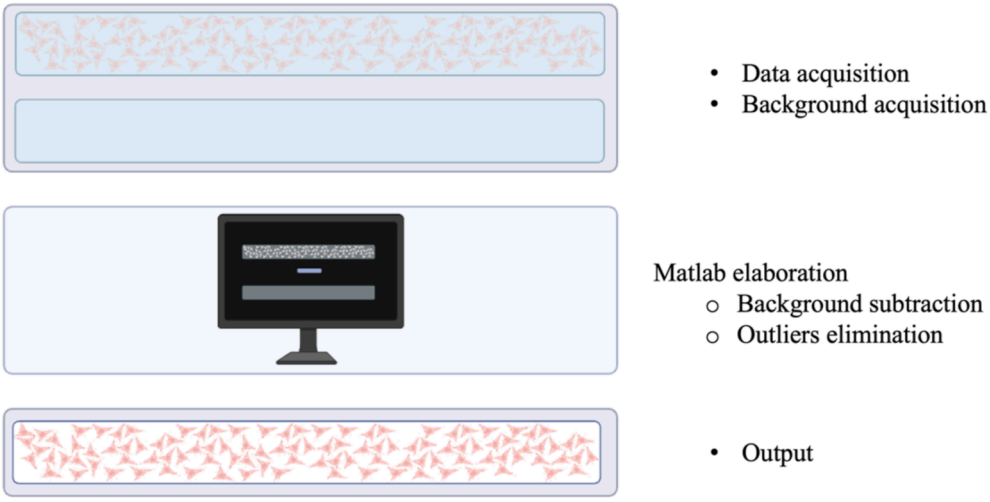

Fig. 1. Schematic representation of the acquisition and analysis of sonoluminescent images.

Fisher Scientific, Waltham, MA, USA) at 450 nm, with 620 nm as the reference wavelength. The values obtained by subtracting 450 nm from 620 nm were further subtracted from the values obtained with ZnO-Lip dispersed in RPMI. The resulting measurements were then compared to those obtained from the control cells.

2.8. Echographic measurements

ZnO and ZnO-Lip nanocrystals were also tested as possible ultrasound nano-contrast agents, first in suspension in two different media (i.e. double distilled water and RPMI) and then injected in an agar phantom. The first measurements were performed exploiting an ultrasound scanner (Ultrasonix Sonix Touch) equipped with a linear array probe (L14-5/38) operating at a frequency of 10 MHz in high resolution B-mode. ZnO and ZnO-Lip NCs were resuspended in 4 mL of double distilled water at a concentration of 100 μg/mL in a plastic cuvette. The solution received an ultrasonic stimulation by the US device (Chattanooga, Intelect Mobile 2 COMBO, DJO France) at power density of 2 W/cm^2 (DC 100 %) and 1 MHz in frequency. The probe was placed under the cuvette and orthogonally with respect to the linear probe of the ultrasound scanner (see scheme in Fig. S2A of the Supporting Information S.I.). The experiment was then repeated resuspending the NCs in cell culture medium, RPMI-1640 supplemented with 10 % heat-inactivated FBS (ATCC), 100 μg/mL streptomycin and 100 units/mL penicillin (Sigma). In both cases, the response to US insonation was analyzed through 30 s real-time videos by the ultrasound scanner.

In a second setup, a research ultrasound scanner (Verasonics Vantage 256) equipped with a linear array (L11-5v, central frequency 10 MHz) was exploited. In this case, 100 μg of ZnO and ZnO-Lip nanocrystals in water suspension (concentration 1 mg/mL) were directly injected into

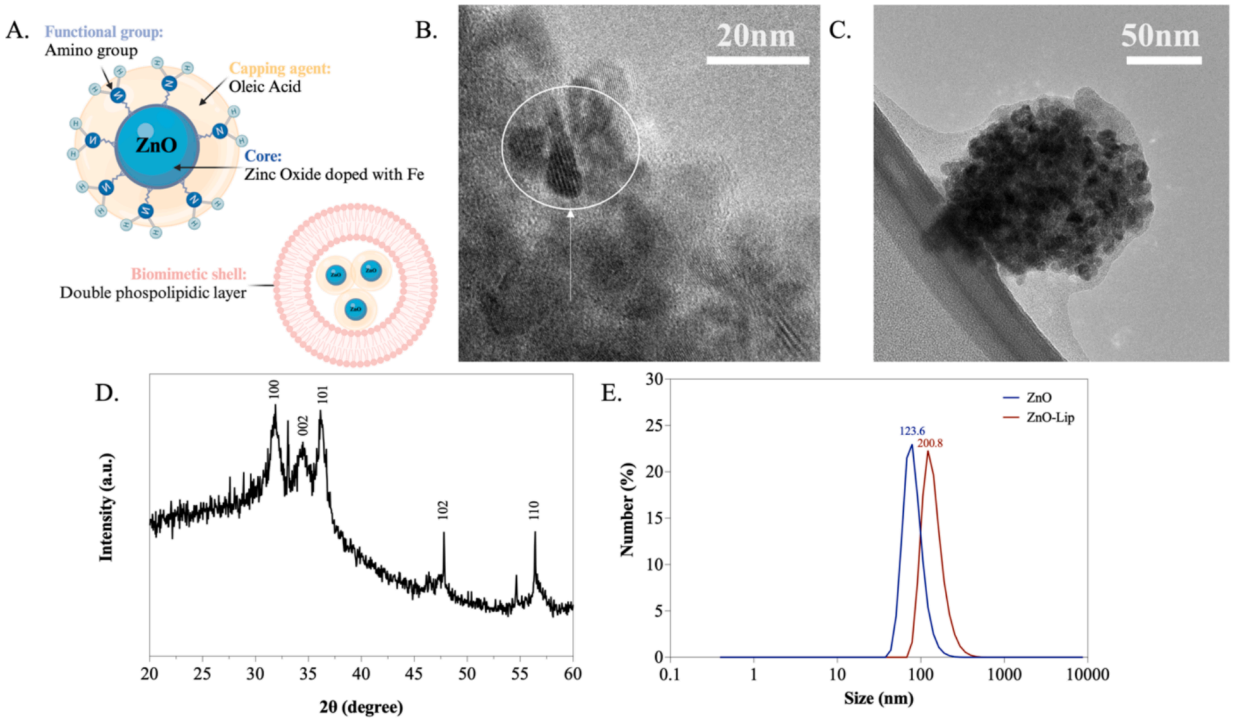

Fig. 2. (A) Schematic representation of ZnO and ZnO-Lip structures and composition. (B) TEM images of ZnO NCs and (C) ZnO-Lip. (D) XRD analysis of ZnO NCs and (E) DLS Number measurement of ZnO and ZnO-Lip in water at the concentration of 100 μg/mL.

an agar phantom, which was placed under the linear probe (Fig. S2B of the S.I.), without any further external stimulation. The same approach was then used to perform the same measurements on an ex-vivo tissue (bovine liver). These adjustments were adopted to better simulate actual operating conditions.

3. Experimental results and discussion

3.1. Nanocrystals characterization

The synthesis of Fe-doped ZnO NCs was performed through an already studied wet chemical method[24], which exploits the oleic acid as capping agent and amino-propyl groups as functionalization compounds, to increase the ZnO colloidal stability (Scheme in Fig. 2A). The ZnO morphology was assessed by HR-TEM analysis, where the ZnO dimension ranges from 8 to 12 nm, and the white circle in Fig. 2B evidences the crystallographic planes obtained from some of the various ZnO crystalline nanostructures. It is of note that the procedure to image these NCs under HR-TEM requires to first dry the suspension of particles on the TEM grid and then image in ultra-high vacuum conditions. Therefore, NCs heavily aggregate on the sample holder. XRD analysis (Fig. 2D) underlines the wurtzitic crystal nature of the synthetized ZnO. The hydrodynamic radius of these Fe-doped ZnO NCs in water is 123.6 nm (Fig. 2E, blue line) with a monodisperse size distribution and a polydispersity index (PDI) of 0.102. Comparing the dimension of the aggregates of ZnO NCs under TEM analysis with DLS results, it is clear that a certain degree of aggregation is also present in water suspension. However, these clustered ZnO NCs are colloidally stable and uniform in size.

The ZnO NCs were encased in a customized lipidic shell (scheme in Fig. 2A), which was formulated in our laboratory inspired to the lipidic formulation of COVID-19 vaccines[28]. The shell was self-assembled on the ZnO NCs to achieve a core–shell hybrid nanoconstruct, showing high bio- and haemo-compatibility and superior colloidal stability of the final nano-agent (ZnO-Lip), as also recently proven by some of us[29]. Low-voltage TEM images (at 60 kV) on freshly-prepared ZnO-Lip (Fig. 2C) allow to see a halo, probably due to the lipidic shell, around a cluster of several NCs. This image, representative among similar ones, confirms the effective encapsulation of a multitude of ZnO NCs inside the lipidic shell. The hydrodynamic radius of ZnO-Lip in water is 200.8 nm, again showing a very uniform and monodispersed size distribution and a PDI of 0.20 (Fig. 2E, red line).

3.2. Bubble cavitation and attenuation measurements

As already verified by some of us [14], the presence of amino-propyl surface functionalization of ZnO contributes to the trapping of gas pockets at the nanocrystal surfaces. This phenomenon aids the use of the NCs as nano-contrast agents for ultrasound imaging. Indeed, the bubble gas pockets trapped on the surface of NCs can induce inertial cavitation, as previously demonstrated from acoustic pulse-echo measurements [14]. Here, we aim to further improve our understanding of the cavitation mechanism by directly characterizing the oscillating bubbles using ultra-high-speed imaging and by indirectly characterizing the bubble size and stability using acoustic attenuation spectroscopy. We therefore immersed the ZnO NCs in water and located the suspension in a microfluidic chamber exposed to ultrasound at a range of acoustic pressure amplitudes, frequencies, and duty cycles (as described in the Materials and Method section). Then we visualized the formation and MHz oscillations of gas bubbles using an ultra-high-speed camera equipped with a 40x magnifying objective. It is worth to note that the ZnO NCs in water tend to create small aggregates, which preferentially arrange in a 1D direction, possibly due to either the transient formation of polar surfaces under the mechanical stimulation of these piezoelectric materials [30] or the self-assembly of these ligand-stabilized NCs [31,32]. Remarkably, Fig. 3A also shows that gas bubbles are already present at the surface of ZnO NCs aggregates prior to the application of ultrasound. When exposed to ultrasound, the micron-sized gas pockets entrapped at the ZnO surfaces coalesce into a bigger micrometer-sized bubble, which is stabilized by the presence of ZnO, as illustrated in

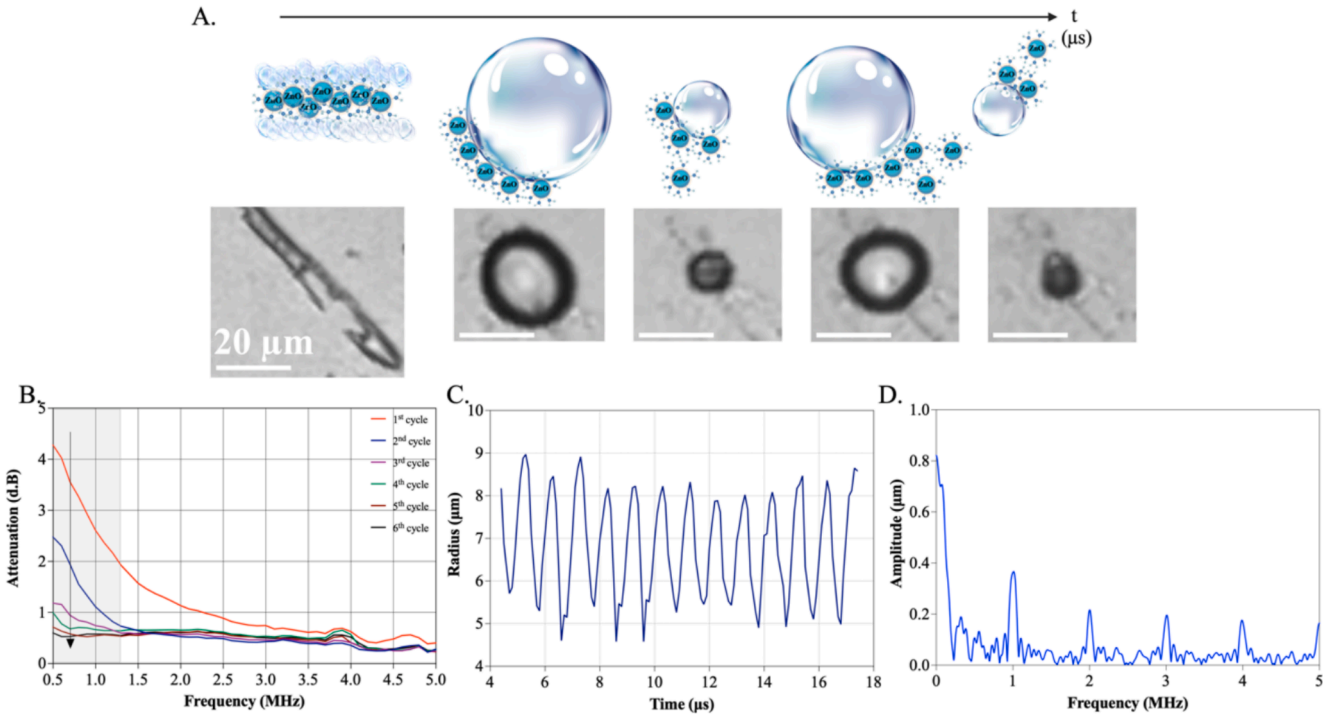

Fig. 3. (A) Schematic representation and ultra-high-speed images of ultrasound driven bubbles, initially trapped at the surface of ZnO particles. (B) Acoustic attenuation spectra measured for a suspension of ZnO NCs at a peak-negative acoustic pressure amplitude of 95 kPa measured successively for 6 times. (C) Bubble radius in time and (D) bubble amplitude in frequency obtained with MATLAB analysis of representative recorded video.

Fig. 3A. Probably, also nano-sized gas pockets are entrapped on NC clusters or even on single NCs, but we can not optically resolve them due to the diffraction limit. The micrometric bubble starts to oscillate, undergoing phases of expansion and contraction, as expected during cavitation. It is worth noting that the ZnO self-assembly in 1D structures governs the initial morphology of the microscopic gas cavity (Fig. 3A, first panel at the left). Then the gas bubbles, while oscillating, coalesce into a single microbubble with a spherical shape, indicating that the bubbles reduce surface energy by coalescing, turning them into a spherical bubble. Its radius then expands and contracts due to the driving ultrasound wave, as observed in the panels in Fig. 3A. Video files of Fig. 3A are provided in the S.I. (Video S.1).

The presence of large micron-sized bubbles in a suspension of ZnO NCs is further supported by the acoustic attenuation spectroscopy measurements shown in Fig. 3B. The figure demonstrates that attenuation was high at the 1st repetition of the attenuation measurements and decreases when the measurement is repeated. This recorded phenomenon witnesses that the bubbles are already present in the ZnO NCs suspension at the beginning and dissolve due to ultrasound driving. Furthermore, the frequency of maximum attenuation (0.5 MHz or lower, see Fig. 3B) provides information on the bubble sizes present in the NCs suspension. Microbubbles are resonators with a characteristic eigenfrequency f_0 that is inversely proportional to the microbubble radius R_0, as given by Minneart's rule of thumb: $f_0 R_0 = 3.3 \mu m MHz$. As the frequency of maximum attenuation approximately equals the resonance frequency of the bubbles, the relatively low frequency of maximum attenuation of 0.5 MHz or lower demonstrates that there were many relatively large microbubbles present with sizes of 6 μm or more in radius. This is consistent with the ultra-high-speed imaging results of which a typical example is shown in Fig. 3C. The figure shows oscillations over time of a microbubble with an equilibrium radius of approximately 7 μm that oscillates at an amplitude of approximately 2 μm (maximum radius of 9 μm in the expansion phase and minimum of 4.5 μm in the contraction phase). The bubble was driven at an ultrasound frequency of 1 MHz. The Fourier Transform of the radius-time curve shown in Fig. 3D indeed shows a strong fundamental response at 1 MHz, but also a strong second, third, fourth, and fifth harmonic demonstrating that the bubble was nonlinearly oscillating under the employed ultrasound driving conditions.

A completely different scenario concerning bubble formation and oscillation is observed when considering a water suspension of our core–shell NCs, i.e i.e. ZnO-Lip, as schematically shown in Fig. 4A. In this case gas bubbles with a diameter beyond the diffraction limit of approx. 0.5 μm are not already present at the ZnO-Lip surface, but bubbles nucleate under ultrasound irradiation. High-speed imaging of ZnO-Lip solution did not portray any pre-existent bubbles that oscillated during the 10 microseconds of the video period. To further underline this, the measured bubble attenuation signal was very low during the first repetitions of the attenuation measurements (Fig. 4B). As opposed to what happens with pristine ZnO NCs, where the attenuation signal decreases during subsequent cycles (Fig. 3B), with ZnO-Lip the acquired attenuation signal begins to increase with the number of insonations. These results suggest that in presence of the core–shell ZnO-Lip NCs the bubbles are either not already present in the solution, or of a diameter below 1 μm, due to the presence of the lipidic shell; they indeed start to nucleate, or grow if they are nano-sized bubbles, over time, and their oscillations, responsible for the establishment of inertial cavitation, is maitained over time. To corroborate this hypothesis, DLS measurements were performed on both ZnO and ZnO-Lip water suspensions before (Fig. 4C) and after (Fig. 4D) the irradiation with ultrasound, at the same condition at which the following sonoluminescent experiments were performed. DLS intensity measurements before US irradiation (Fig. 4C) show two clear size distribution peaks (138 nm for ZnO NCs suspension and 200.8 nm for ZnO-Lip NCs one), reporting homogeneous size distributions. The larger dimension of the ZnO-Lip suspension with respect to ZnO NCs is consistently attributed to the presence of lipidic coating. After ultrasound irradiation for 120 s, both ZnO and ZnO-Lip suspensions display different DLS intensity curves (Fig. 4D). In the ZnO NCs distribution curve, a single peak is still visible, but at higher diameter (275.2 nm), meaning that a further aggregation of NCs occurred after US application. In the ZnO-Lip size distribution curve, two different peaks are present: one at a slightly larger dimension (217 nm) than before US application and one at a large dimension (784 nm). We can assume that aggregation of the ZnO-Lip can occur due to the US application, but more probably this last peak at such low %intensity value can indicate the re-assembly of lipids, due to the ultrasound irradiation, forming a lipid shell around gas bubbles, thereby stabilizing them.

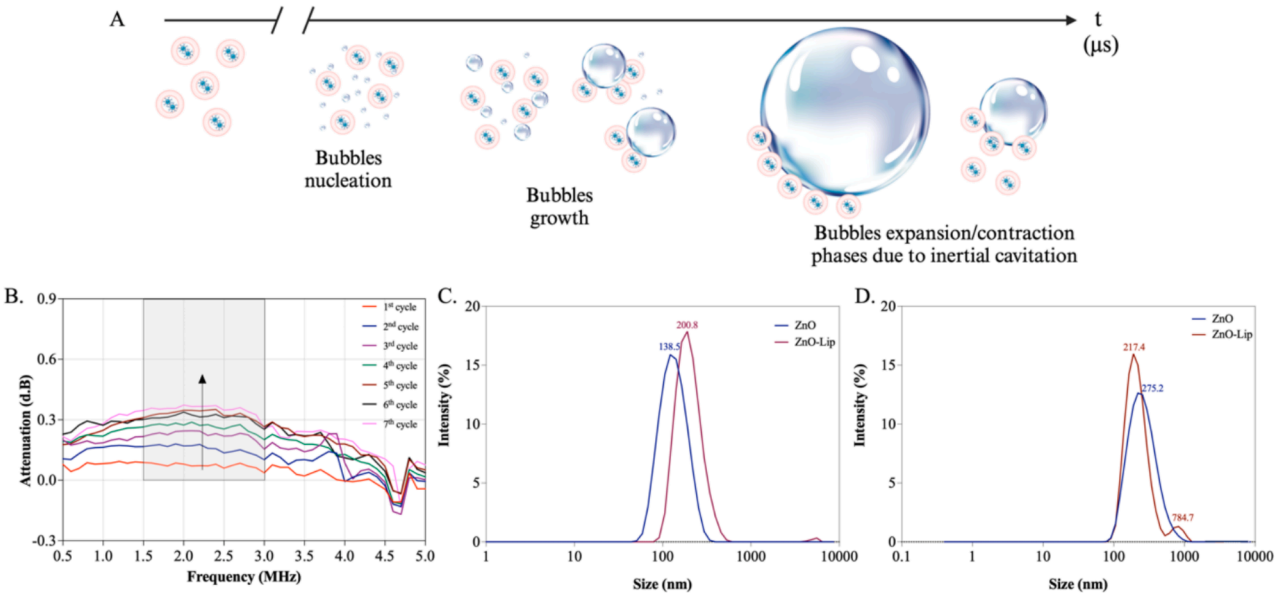

Fig. 4. (A) Schematic representation and recorded images of bubble dynamics in presence of ZnO-Lip. (B) Bubble attenuation signals in presence of ZnO-Lip at 95 kPa measured in subsequent pressure cycles. DLS Intensity measurement of ZnO and ZnO-Lip (C) pre and (D) post 120 s of ultrasound exposure at 2 W/cm^2, 1 MHz, 100 % DC.

3.3. Sonoluminescence measurements

After characterizing the bubble dynamics in combination with ZnO and ZnO-Lip NCs following ultrasonic stimulation, the focus is now on evaluating the intensity of light emission produced by inertial cavitation. The first recordings of sonoluminescence were conducted in water (Fig. 5) in the presence and absence of ZnO and ZnO-Lip at different concentrations. The image obtained with ultrasound stimulation in pure water was normalized as described in the Materials and Method section, resulting in an image with all pixels at 0 for the reference case (Fig. 5A). This normalization was performed because the objective of this experiment was to observe the sole influence of the nano-sized contrast agents, ZnO and ZnO-Lip NCs, on the intensity of sonoluminescence. As such, the value of the pure water image (background) was subtracted from all the images further acquired (Fig. 5B-E). Comparing these captured light images and pixel intensity distributions (Fig. 5F), a trend in the amount of collected light, as well as in pixel intensity distribution, is visible, clearly dependent on the concentration of nano-contrast agents present in solution. ZnO NCs at 100 μg/mL are able to contribute in generating, under US insonation, a lower amount of photons compared to the same suspension at 200 μg/mL (Fig. 5G). The same behavior can be visualized for ZnO-Lip NCs (Fig. 5H): at a concentration of 200 μg/mL a higher pixel intensity distribution is achieved in comparison to a concentration of 100 μg/mL. Similarly, the collected images clearly depict a brighter intensity in Fig. 5E, collected using ZnO-Lip at 200 μg/mL, with respect to Fig. 5D, adopting a ZnO-Lip at 100 μg/mL. These results underline once again the pivotal contribution given by both ZnO and ZnO-Lip NCs as nano-contrast agents, yet augmenting the sonoluminescent light generation under ultrasound insonation. The above results demonstrate how the phenomenon is directly dependent on the nano-contrast agent concentration: by increasing it, an increase in the production and subsequent collection of SL photons is clearly evident.

Interestingly, the presence of the lipidic coating on the ZnO seems to greatly enhance the sonoluminescent light generation: by comparing the pixel distributions of ZnO and ZnO-Lip NCs at both concentrations (Fig. 5I and J), the higher contribution given by ZnO-Lip with respect to ZnO is evident. It can be assumed that the inertial cavitation phenomenon is endured and consequently the generated sonoluminescent light. As discussed above (Fig. 4), the micrometer sized gas bubbles at the surface of ZnO-Lip are not present from the beginning, due to the hydrophilic polar heads of the lipidic shell. The results indicate that inertial cavitation and related gas bubbles grow in size with time, favored by the nucleation of new gas bubbles. Furthermore, these bubbles seem to coalesce and be stabilized by the ultrasound-mediated re-assembly of lipids that compose the lipidic shell, as revealed by the DLS measurement in Fig. 4D. As DLS and SL experiments were conducted at the same US irradiation conditions, the data suggests that the increase of SL light intensity is due to the presence of the large bubbles, stabilized by the lipids, which leads to sustained cavitation, causing a sustained sonoluminescence over time. Indeed, the images of Fig. 5 are acquired over a large time window (120 s) and the captured light is higher in the presence of ZnO-Lip NCs.

On the contrary, the gas bubbles at the ZnO surface are already present in solution, before the US insonation (Fig. 3). Thus, the main contribution to the sonoluminescent phenomenon is given by these bubbles, that coalesce, implode, and dissolve in a short amount of time.

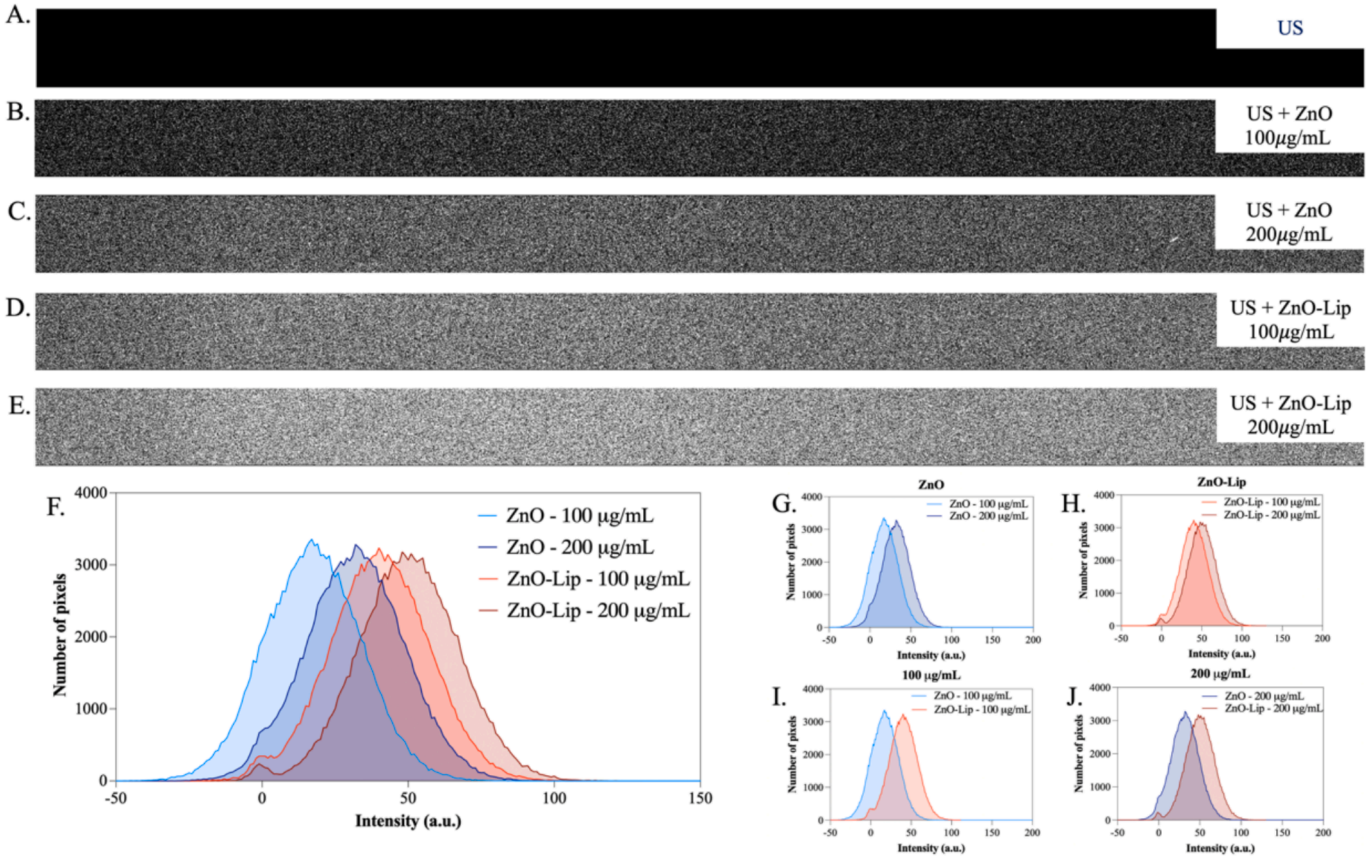

Fig. 5. (A) Sonoluminescence signal obtained in pure water and water in presence of ZnO with a concentration of (B) 100 μg/mL and (C) 200 μg/mL, and in presence of ZnO-Lip with a concentration of (D) 100 μg/mL and (E) 200 μg/m. The sonoluminescence signal of pure water irradiated with US was subtracted as background from each image. Intensity pixel distribution of all the sonoluminescence images obtained with (F) ZnO and ZnO-Lip, of the images obtained with (G) different concentration of ZnO, of the images obtained with (H) different concentration of ZnO-Lip, of the images obtained with (I) 100 μg/mL of ZnO and ZnO-Lip and of the images obtained with (J) 100 μg/mL of ZnO and ZnO-Lip. Each tested solution was irradiated for 120 s with 2 W/cm^2, 1 MHz and 100 %DC.

Among others, one of the aims of this work is to open new horizons and discover new possibilities for the application of sonoluminescence augmented by biocompatible nanocrystals, i.e. ZnO-Lip, in the biomedical field, particularly for bio-imaging purposes.

Moving toward this direction, the sonoluminescence generation tests were repeated in a biologically-relevant medium, i.e. one of the most common cell culture media, RPMI-1640 completed with 10 % FBS. In this case, results (Fig. 6) are dissimilar to the water ones, but in accordance with the assumptions verified in a previous work [19]. More in detail, it was observed that the intensity of the emitted light signal in media rich in proteins and biomolecules, decreases compared to liquids like water, due to the different absorption of light of such macromolecules, absent in bi-distilled (b.d.) water.

The brightness of the acquired images (Fig. 6B-E) is clearly lower with respect to the images acquired in b.d. water at the same conditions (Fig. 5), confirming previous findings in the literature[19]. Still, trends can be identified. Considering the suspension in RPMI, the sonoluminescent signal obtained with the concentration of 100 μg/mL is clearly lower than 200 μg/mL concentration (Fig. 6 B, C G), as similarly reported in water. Conversely, the same trend cannot be obtained with ZnO-Lip NCs suspensions (Fig. 6 D, E and H), where same intensity of sonoluminescent light was generated at both concentrations. Comparing the data acquired with either ZnO or ZnO-Lip NCs at 100 μg/mL, an increase of the generated photons is remarkable (intensity pixel distribution in Fig. 6I). However, the same trend is not evident when comparing ZnO and ZnO-Lip NCs at 200 μg/mL concentration (Fig. 6J).

Whilst the results in RPMI generally demonstrate the decrease of the intensity of generated photons, the contribution given by the ZnO-Lip NCs, even at low concentration i.e. 100 μg/mL, is clearly evident in enhancing the brightness of the sonoluminescent image with respect to the ZnO NCs.

The complexity of the medium, rich in macromolecules which can absorb photons or displace gas bubbes, can contribute to set a maximum number of cavitation bubbles that can implode and generate SL light. This can be the reason behind the lack of difference between the signal recorded with ZnO-Lip at 100 μg/mL and 200 μg/mL, where the highest contribution in enhancing the SL is already given with a concentration of 100 μg/mL.

According to these data, ZnO-Lip at a concentration of 100 μg/mL was the condition chosen for further in vitro experiments. ZnO-Lip are more biocompatible with respect to pristine ZnO[28], and the condition of 100 μg/mL of ZnO-Lip is the one which allows to obtain the highest signal with the lowest tested concentration.

In vitro colorectal adenocarcinoma cells (HT-29 cell line) were thus cultured with 100 μg/mL of ZnO-Lip (Fig. 7). Optical images of the inverted microscope (using a 60x objective and a cooled CCD) were initially recorded in presence of ambient light (Fig. 7A) or in dark condition with only the contribution of SL photons under ultrasound irradiation (Fig. 7B). In this last case, it is possible to clearly distinguish the shape of some cells when SL photons were acquired. Despite this is the first time ever, to the authors' knowledge, that an image of a living cell is obtained with the sole use of sonoluminescence, this image is less detailed than the one acquired with ambient white light (Fig. 7A). The greatest outcome was achieved in the presence of the core–shell ZnO-Lip

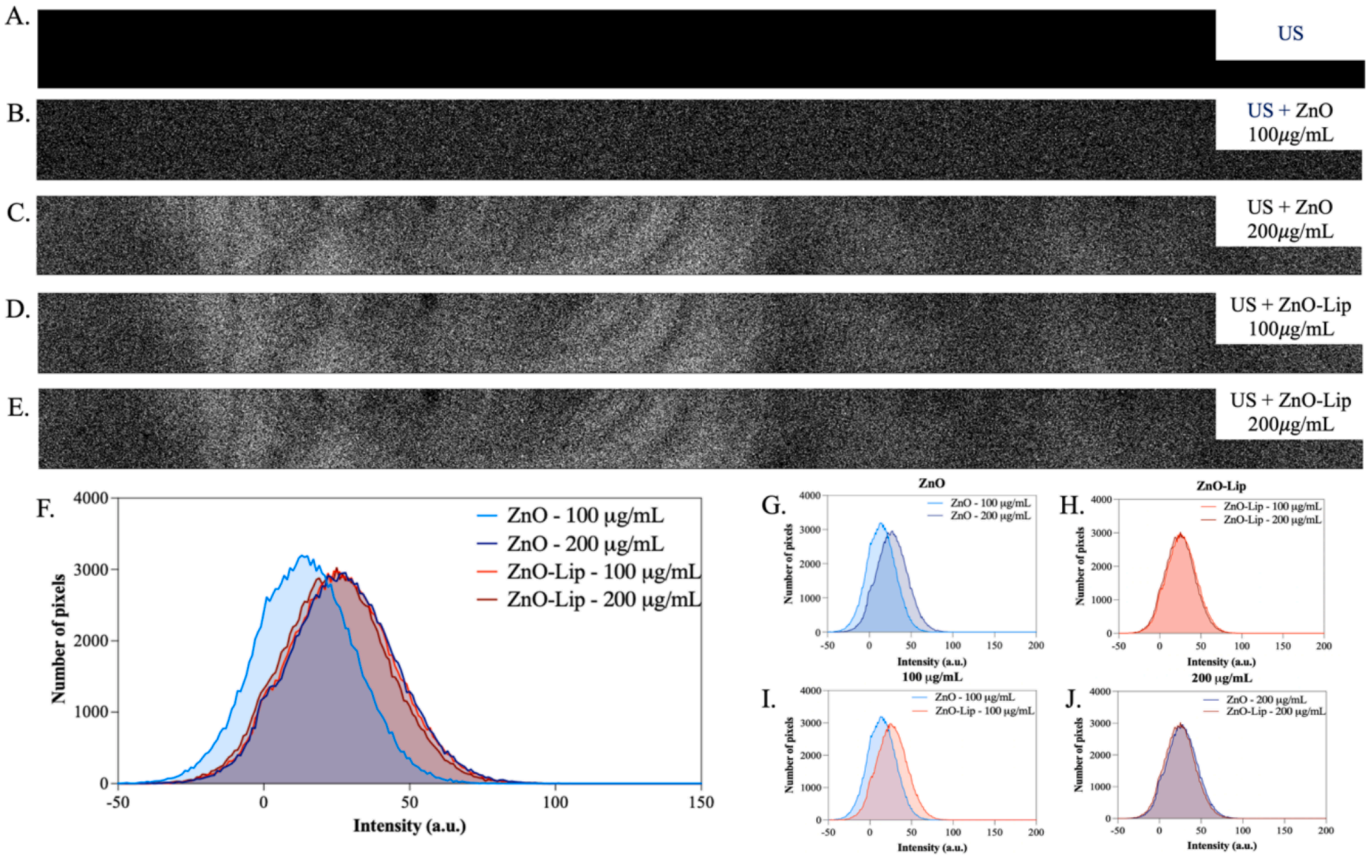

Fig. 6. (A) Sonoluminescence signal obtained in complete RPMI cell culture medium, and complete RPMI cell culture medium in presence of ZnO with a concentration of (B) 100 μg/mL and (C) 200 μg/mL, and in presence of ZnO-Lip with a concentration of (D) 100 μg/mL and (E) 200 μg/m. The sonoluminescence signal of pure water irradiated with US was subtracted as background from each image. Intensity pixel distribution of all the sonoluminescence images obtained with (F) ZnO and ZnO-Lip, of the images obtained with (G) different concentration of ZnO, of the images obtained with (H) different concentration of ZnO-Lip, of the images obtained with (I) 100 μg/mL of ZnO and ZnO-Lip and of the images obtained with (J) 100 μg/mL of ZnO and ZnO-Lip. Each tested solution was irradiated for 120 s with 2 W/cm^2, 1 MHz and 100 %DC.

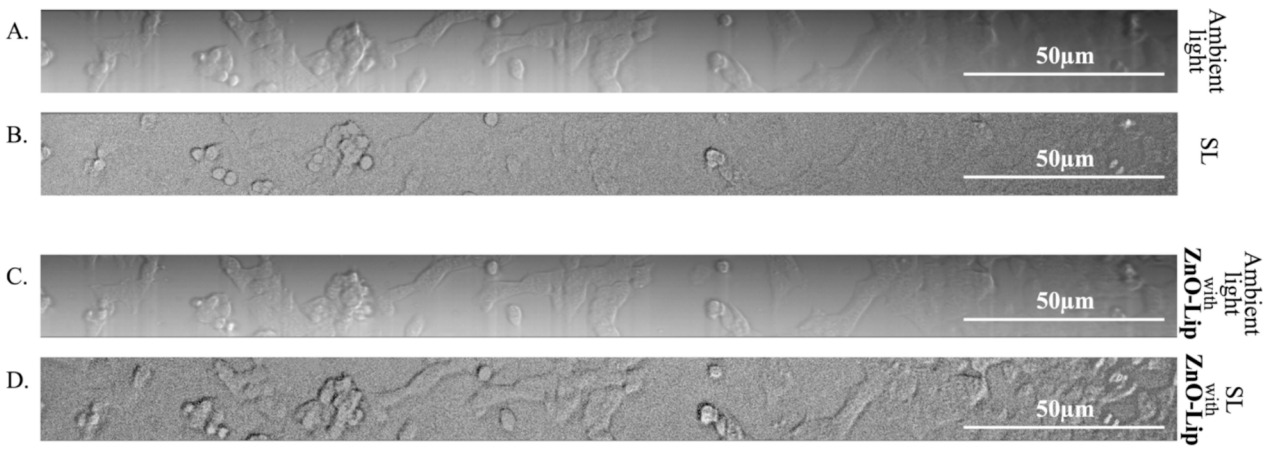

Fig. 7. HT-29 cells, in complete RPMI cell culture medium, captured by CCD camera after 120 s of acquisition. (A) and (C) show the images of cells acquired with ambient light, (B) is obtained in the dark thank to the sonoluminescent (SL) signal, and (D) is obtained in the dark thank to the light emitted by the sonoluminescent phenomenon augmented by the presence of 100 µg/mL of ZnO-Lip. Samples (B) and (D) were irradiated for 120 s with 2 W/cm^2, 1 MHz and 100 %DC.

NCs (Fig. 7D): they really act as a contrast agent allowing to achieve a clearly defined, bright and well-detailed image. In the provided image, it is possible to easily discriminate all cell borders, with the same or even superior details available and an increased definition than the ones achieved with ambient white light (see Fig. 7A and C for comparison). Indeed, ZnO-Lip NCs allow to generate a large number of photons, due to the cavitation maintained over time.

The above impressive results prove the applicability of an innovative, original and safe (as reported in the S.I., Fig. S3) method of in vitro imaging. To the authors' knowledge, this is the first example of in vitro living cancer cell line images ever obtained only through photons generated by sonoluminescence and augmented by the presence of biocompatible ZnO-Lip nano-contrast agent at a not-toxic concentration, i.e. 100 µg/mL[28].

3.4. Contrast-Enhanced ultrasound imaging with NCs

In addition to the previous findings on SL, we also evaluated the possible role of both ZnO and ZnO-Lip when applied as nano-contrast agent for ultrasound imaging. Here, the well-known B-mode ultrasound imaging technique was exploited (Fig. 8), challenged with the additional use of the NCs. Firstly, a cuvette filled with b.d. water was subjected to an external ultrasound stimulation and its response to such stimulus was evaluated through a live video recording. Then, ZnO and ZnO-Lip were separately added to the solution to investigate their role in the contrast enhancement in the ultrasound image. The same procedure was repeated by replacing b.d. water with RPMI. The images in Fig. 8 report some significant and representative frames taken from the live videos. As clearly visible, the presence of both ZnO or ZnO-Lip NCs increases the contrast of the image, confirming the possibility of exploiting these nanocrystals also as ultrasound contrast agents. In particular, in the case of a water-based solution (Fig. 8A), despite the highest contrast is achieved with ZnO NCs (central panel), a more defined and clearer signal is achieved with ZnO-Lip suspension (right panel) compared to the blurred image collected with ZnO NCs.

Concerning the cell culture-based solution (Fig. 8B), the best contrast result is obtained with ZnO-Lip NCs (right panel) while no signal can be recorded when using the ZnO NCs (central panel), thus confirming again the superior contrast-enhanced effect of the core–shell NCs

It is worth noting that the above measurements were produced by insonation of the suspensions of water and RPMI with an external ultrasound source at low frequency (i.e. 1 MHz) and collecting the images with the ultrasound imaging probe at 10 MHz (for details of the set up see Fig. S2A of the S.I.). To approach the actual operating conditions of a real scenario, a second set of measurements was carried out by using the ultrasound imaging probe at 10 MHz only. The echographic signal was analyzed from a mock tissue, adopting with a penetration detection from 2 to 4 cm and using ZnO or ZnO-Lip suspensions as contrast agents, or simple double distilled water as control media (Fig. 9).

Interestingly, two important results are observed: firstly, it is not needed to externally stimulate the setup with a separate ultrasound source (i.e. the one at 1 MHz as above), since a highly positive contrast can be obtained just by exploiting the echographic probe (operating frequency used here 10 MHz); secondly, we observed a sustained-over-

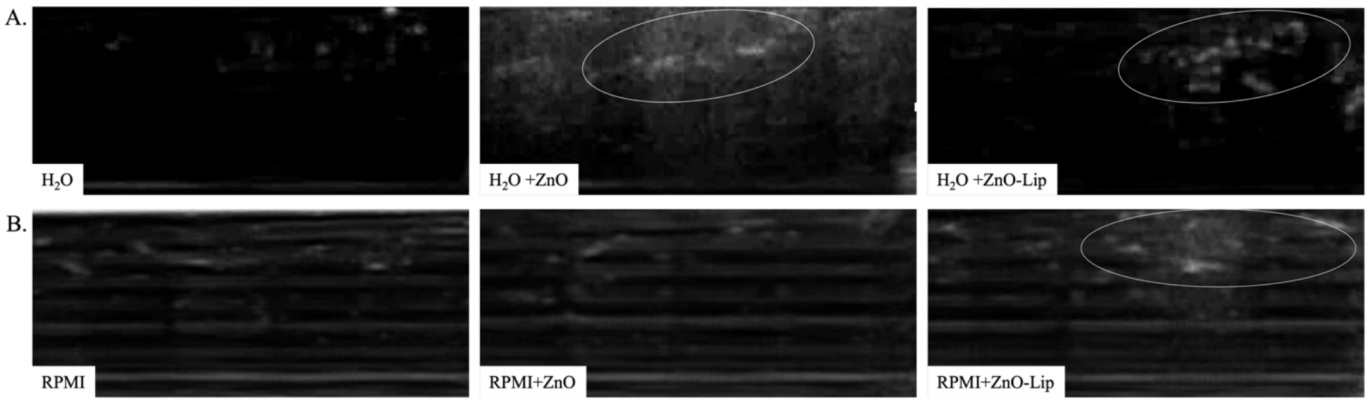

Fig. 8. (A) Echographic contrast signal of water, water with 100 µg/mL of ZnO and ZnO-Lip and (B) complete growth medium, i.e. RPMI, RPMI with 100 µg/mL of ZnO and ZnO-Lip when irradiated with ultrasound equal to 2 W/cm^2, 1 MHz and 100 % DC. White circles indicated the areas with the highest contrast signal.

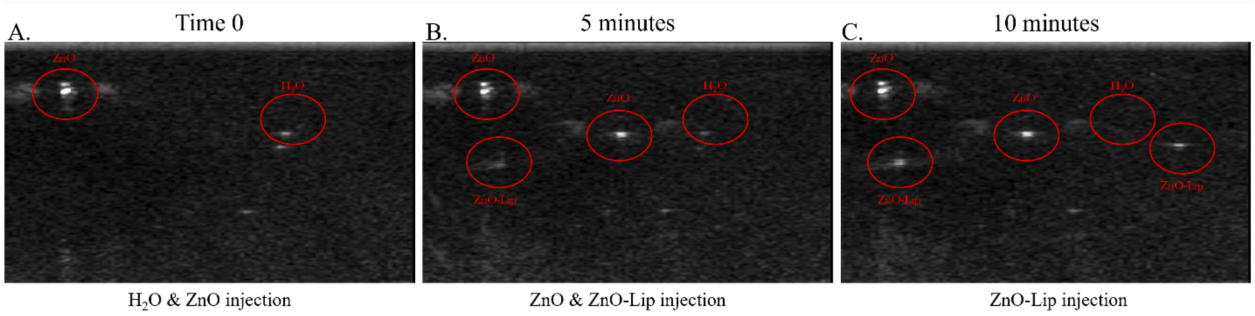

Fig. 9. Echographic contrast signal of a mock tissue injecting water (at time 0), ZnO suspension (at time 0 and at minute 5) and ZnO-Lip suspension (at minutes 5 and 10). The analysis over time at (A) time 0, (B) after 5 min, and (C) after 10 min allowed to evaluate the signal persistence.

time contrast imaging, which lasts for several minutes when injecting in the mock tissue the suspension of either ZnO or ZnO-Lip nanocrystals (see the comparison among the red circles in Fig. 9 from A to C). In case of simple water injection, the contrast is visible, but then immediately lost. Concerning the contrast enhancement, the highest one is obtained with ZnO, with the one derived from the use of ZnO-Lip being slightly lower, but also sustained over time.

To get even closer to real operating conditions, the same setup was exploited to analyze the echographic signal of an ex-vivo tissue (Fig. 10). Also in this case, the contrast given by the water injection is almost irrelevant, especially if compared to that obtained after the injection of ZnO and ZnO-Lip suspensions, which is on the contrary extremely evident. This difference is indeed more noticeable when observing the live videos of the injections, reported in the S.I. (Video 2). These results are in line with the ones derived from the agar phantom analysis, thus corroborating the idea that ZnO and ZnO-Lip NCs could be exploited as effective nano-contrast agents in a more realistic scenario.

4. Discussion

This work aims to unveil new perspectives on the biomedical imaging application of sonoluminescence. We have reported two different bio-imaging approaches where ultrasound is exploited and the effects augmented by the presence of NCs suspensions are studied. Notably, we have adopted two nanocrystals formulations, i.e. ZnO NCs and lipid-coated NCs (ZnO-Lip). From a biocompatibility perspective, it is well known that pristine ZnO micro and nanomaterials cannot be safe, and we and others have reported the concentration-dependent cytotoxicity of this material[33]. In contrast, high bio-, cyto- and hemo-compatible behavior are achieved when coating the presented ZnO NCs with a biomimetic phospholipidic bilayer shell[17,18]. Thus, the safety of this ZnO-Lip nanomaterial empowers us for its use in diverse nanomedicine applications, from bio-imaging and diagnosis to therapeutic interventions. Remarkably, we have previously shown that ZnO-Lip are useful up to 100 μg/mL, the same concentration adopted in the present work, to be activated by repetitive acoustic shock waves or ultrasound stimulations and trigger a convenient cancer cell killing. This effect is even more pronounced when conjugating a targeting ligand (peptides [28], antibodies[34] or fragmented antibodies[20]) to the lipid bilayer shell, allowing a site selective internalization and cell killing of cancer cells up to 3D spheroids while sparing healthy ones[20,29]. These effects are summarized in Table 1. In contrast, pristine ZnO NCs cannot be used at the same concentration for this therapeutic purpose as they are intrinsically toxic and we have previously reported their combination at very low concentrations (i.e. up to 5–10 μg/mL[35]) with shock waves, as reported in Table1.

We have also demonstrated that after 24 h of incubation with cells, both types of nanocrystals are conveniently internalized into cells, specifically in cancer ones[20,21,28,29,35,36]. With the results demonstrated in the present paper, we can argue that once the ZnO-Lip NCs are internalized in cells at relevant timing, the produced cavitation bubbles due to US irradiation are likely to be generated from the cell interior, potentially explaining the resulting production of ROS and mechanical damages we have already observed[20,29,35,36] and ultimately leading to cell death.

By matching the therapeutic effect of NP-assisted US together with the bio-imaging potentialities proposed here we can conceive a full theranostic nano-sized platform activated by ultrasound. We envision indeed that with ZnO-Lip assisted SL we can visualize in vitro cultured cells before and after treatment, and then evaluate the final efficacy of the US-therapeutic treatment when ZnO-Lip are administered at the same concentration used for the prior visualization. As we have demonstrated above, the role of inertial cavitation of gas bubbles has a pivotal role for the SL imaging (and echography) as well as for inducing

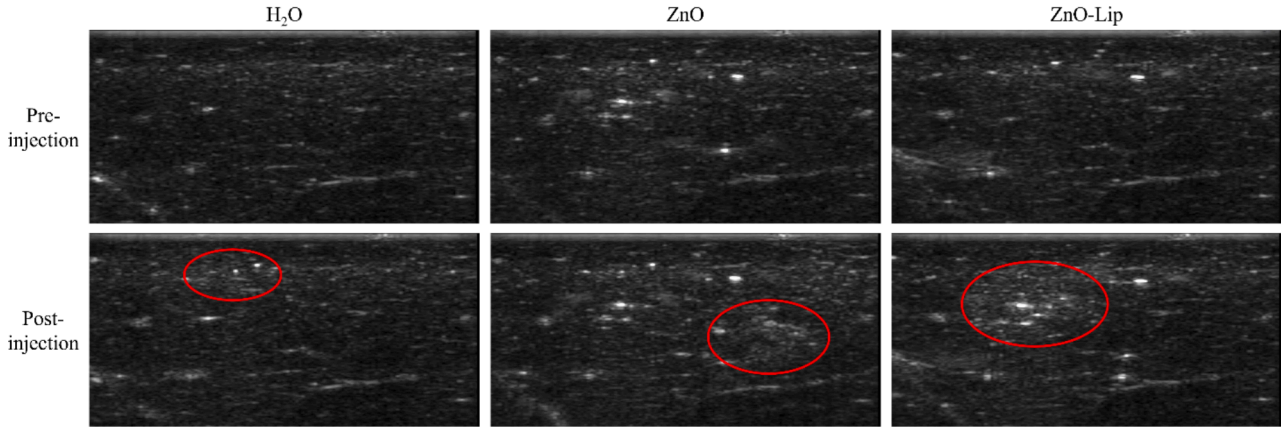

Fig. 10. Echographic contrast signal of an ex-vivo tissue pre and post injection of water, and ZnO and ZnO-Lip suspensions.

Table 1
Previous results obtained by the authors which demonstrate the efficacy of ZnO (with and without lipidic shell and targeting agent) combined with acoustic waves for the treatment of different types of cancers.

Disease	Nanoconstruct	Targeting agent	Concentration	Pressure waves source	Treatment Protocol	Ref.
Colorectal cancer (2D culture)	Lipid coated iron doped ZnO	YSA peptide	50 μg/mL	Shock waves (250 shots, 0.22 or 0.35 mJ/mm^2)	3 treatments, 1 treatment per day	[29]
Colorectal cancer (3D spheroid)	Lipid coated iron doped ZnO	YSA peptide	100 μg/mL	Shock waves (250 shots, 0.22 or 0.35 mJ/mm^2)	3 treatments, 1 treatment per day	[29]
Osteosarcoma (2D culture and 3D spheroid)	Lipid coated iron doped ZnO	YSA peptide	20 μg/mL	US (1.0 and 2.0 W/cm^2, 1 MHz, 100 %DC, 1 min)	1 treatment	[36]
Burkitt's Lymphoma (2D culture)	Lipid coated iron doped ZnO	Fragmented anti-CD38 antibody	40 μg/m	US (0.3 and 0.45 W/cm^2, 1 MHz, 100 %DC, 1 min)	1 treatment	[20]
Colorectal cancer (2D culture)	Iron doped ZnO	–	10 μg/ml	Shock waves (250 shots, 0.12 mJ/mm^2)	3 treatments, 1 treatment per day	[35]
Pancreatic ductal adenocarcinoma(2D)	Iron doped ZnO	–	15 μg/mL	Shock waves (500 shots, 0.04 mJ/mm^2)	1 treatment	[21]
Cervical Adenocarcinoma	ZnO	–	5 μg/mL	Shock waves (500 shots, 0.30 mJ/mm^2)	3 treatments, 1 treatment every 3 h	[22]
Burkitt's Lymphoma	Extracellular vesicles loaded with ZnO	Anti-CD20 antibody	5 μg/mL	Shock waves (250 shots, 0.04 mJ/mm^2)	3 treatments, 1 treatment every 3 h	[34]

therapeutic effects, i.e. the ROS generation and mechanical damage (the "nanoscalpel effect").

In presence of ZnO, we have found that gas bubbles are entrapped at the nanocrystal surface, and when US is applied, they start to coalesce, obtaining oscillating bubbles with a diameter range from 2.5 μm to 5 μm, before imploding and dissolving. On the other hand, with ZnO-Lip, the lipidic shell prevents the entrapment of bubbles on the nanocrystals surface, while the lipidic shell re-assembles itself over time upon US insonation. This lipid reassembly enables the stabilization of gas bubbles, nucleating during US exposure, and generates the bubble oscillations (maintained over time) as indirectly observed from sonoluminescence and echography measurements. According to these dynamics, it is possible to distinguish two behaviors between ZnO and ZnO-Lip suspensions. During short amounts of time, ZnO gives a higher contrast signal, as visible in contrast-enhanced ultrasound measurements in a simple water solution, because of the nature of bubbles. These bubbles are indeed already present and start to oscillate and implode as soon as the US is turned on. The signal, which arose from them is short lived. The results are widely different in the presence of ZnO-Lip. Gas bubbles start to nucleate over time on the short μs time scale, as demonstrated by the absence of oscillating bubbles in the ultra-high-speed video recordings, and by slightly reduced echographic signal intensities recorded with ZnO-Lip in water solution. At longer minute time scale, the results obtained with ZnO-Lip are notable due to the onset of inertial cavitation maintained over time. Furthermore, the sonoluminescent signal, which is recorded during 120 s of CCD exposure, is so high that, for the first time, it enables the in vitro visualization of cells with a higher definition than the ambient light.

We remark however that SL, being a visible light emission, can be used for in vitro bio-imaging only and thus explored for research-based applications. In view of clinically-relevant investigations, we envision the prominent role of echography adopting the proposed ZnO-Lip NCs as nanosized-contrast agents. In this scenario, a targeted ZnO-Lip can be of course beneficial to visualize the disease of interest with micro-meter size resolution, together with the enhanced, long-lasting and in-depth contrast ultrasound imaging.

5. Conclusion

This work describes the dynamics of bubbles under ultrasound insonation when combined with inorganic nanocrystals, i.e. ZnO NCs, and advanced core–shell lipid-coated nanocrystals (ZnO-Lip), as possible contrast agents under biomedical sonoluminescence and ultrasound imaging.

These findings open new horizons for bioimaging applications based on sonoluminescence photons produced in water or biological solutions. The data are augmented by biocompatible ZnO-Lip, confirming the possibility of exploiting such material as efficient contrast agent for SL and ultrasound imaging measurements and even obtain a fully theranostic tool if combined with repetitive ultrasound or shock waves for cancer cell killing.

This scenario offers numerous fields of future interventions and pave the way for proposing a fully theranostic an highly safe nanotool for possible early diagnosis of oncological disease and their prompt treatment.

Fundings

This work has received funding from the European Research Council (ERC) under Grant agreement No. 101081529-Project Acronym "AI CUrES"—ERC Proof of Concept Grant 2021 (V.C.) and under Grant agreement No. 101078313—Project Acronym "MICOMAUS"—ERC Starting Grant 2022 (T.S.), from the National Recovery Plan PNRR – M4C2 – AVVISO 3277/2021 – NODES – ECS00000036 – PoC Nano-Zoom Spoke 5 (V,C,), and from the Italian Ministry of University and Research (MUR) PRIN project 2020MHL8S9 "MITHOS" (V.C.), and Next Generation EU (V.C. and E. P.).

CRediT authorship contribution statement

V. Vighetto: Writing – original draft, Visualization, Validation, Methodology, Investigation, Formal analysis, Data curation. **E. Pascucci:** Writing – review & editing, Visualization, Validation, Investigation. **N.M. Percivalle:** Writing – original draft, Visualization, Methodology, Investigation. **A. Troia:** Writing – review & editing, Supervision, Methodology, Data curation, Conceptualization. **K.M. Meiburger:** Writing – review & editing, Validation, Methodology, Investigation. **M.R.P. van den Broek:** Validation, Investigation. **T. Segers:** Writing – review & editing, Supervision, Resources, Project administration, Methodology, Funding acquisition. **V. Cauda:** Writing – review & editing, Supervision, Resources, Project administration, Funding acquisition, Conceptualization.

Declaration of competing interest

The authors declare the following financial interests/personal relationships which may be considered as potential competing interests: Valentina Cauda reports financial support was provided by European Commission. Valentina Cauda reports financial support was provided by Ministry of Economy and Business. Valentina Cauda reports financial support was provided by Ministry of Education. Tim Segers reports financial support was provided by European Commission. If there are other authors, they declare that they have no known competing financial interests or personal relationships that could have appeared to influence

the work reported in this paper.

Appendix A. Supplementary data

Supplementary data to this article can be found online at https://doi.org/10.1016/j.ultsonch.2025.107242.

References

[1] D.A. Mankoff, A Definition of Molecular Imaging, accessed September 23, 2024, J. Nucl. Med. 48 (2007) 18N–21N, https://jnm.snmjournals.org/content/48/6/18N.

[2] J. Condeelis, R. Weissleder, In vivo imaging in cancer, Cold. Spring. Harb. Perspect. Biol. 2 (2010), https://doi.org/10.1101/CSHPERSPECT.A003848.

[3] X. Han, K. Xu, O. Taratula, K. Farsad, Applications of Nanoparticles in Biomedical Imaging, Nanoscale 11 (2019) 799, https://doi.org/10.1039/C8NR07769J.

[4] Z. Jiang, M. Zhang, P. Li, Y. Wang, Q. Fu, Nanomaterial-based CT contrast agents and their applications in image-guided therapy, Theranostics 13 (2023) 483, https://doi.org/10.7150/THNO.79625.

[5] M. Rahman, Magnetic resonance imaging and iron-oxide nanoparticles in the era of personalized medicine, Nanotheranostics 7 (2023) 424, https://doi.org/10.7150/NTNO.86467.

[6] Y. Chen, S. Wang, F. Zhang, Near-infrared luminescence high-contrast in vivo biomedical imaging, Nat. Rev. Bioeng. 2023 1:1 1 (2023) 60–78. https://doi.org/10.1038/s44222-022-00002-8.

[7] W. Choi, B. Park, S. Choi, D. Oh, J. Kim, C. Kim, Recent advances in contrast-enhanced photoacoustic imaging: overcoming the physical and practical challenges, Chem. Rev. 123 (2023) 7379–7419, https://doi.org/10.1021/ACS.CHEMREV.2C00627.

[8] J.C. Hsu, Z. Tang, O.E. Eremina, A.M. Sofias, T. Lammers, J.F. Lovell, C. Zavaleta, W. Cai, D.P. Cormode, Nanomaterial-based contrast agents, Nat. Rev. Methods Primers 2023 3:1 3 (2023) 1–21. https://doi.org/10.1038/s43586-023-00211-4.

[9] S. Rahmati, A.E. David, A review of design criteria for cancer-targeted, nanoparticle-based MRI contrast agents, Appl. Mater. Today 37 (2024) 102087, https://doi.org/10.1016/J.APMT.2024.102087.

[10] Y. Zhou, X. Han, X. Jing, Y. Chen, Construction of Silica-Based Micro/Nanoplatforms for Ultrasound Theranostic Biomedicine, Adv. Healthc. Mater 6 (2017), https://doi.org/10.1002/ADHM.201700646.

[11] SonoVue | European Medicines Agency (EMA), (n.d.). https://www.ema.europa.eu/en/medicines/human/EPAR/sonovue (accessed September 23, 2024).

[12] S. Zullino, M. Argenziano, I. Stura, C. Guiot, R. Cavalli, From micro- to nano-multifunctional theranostic platform: effective ultrasound imaging is not just a matter of scale, Mol. Imaging 17 (2018), https://doi.org/10.1177/1536012118778216.

[13] M. Wu, W. Chen, Y. Chen, H. Zhang, C. Liu, Z. Deng, Z. Sheng, J. Chen, X. Liu, F. Yan, H. Zheng, Focused ultrasound-augmented delivery of biodegradable multifunctional nanoplatforms for imaging-guided brain tumor treatment, Adv. Sci. (weinh) 5 (2018), https://doi.org/10.1002/ADVS.201700474.

[14] A. Ancona, A. Troia, N. Garino, B. Dumontel, V. Cauda, G. Canavese, Leveraging re-chargeable nanobubbles on amine-functionalized ZnO nanocrystals for sustained ultrasound cavitation towards echographic imaging, Ultrason. Sonochem 67 (2020) 105132, https://doi.org/10.1016/J.ULTSONCH.2020.105132.

[15] L.A. Crum, Resource Paper: Sonoluminescence, J. Acoust. Soc. Am 138 (2015) 2181, https://doi.org/10.1121/1.4929687.

[16] L.V. Wang, Q. Shen, Sonoluminescent tomography of strongly scattering media, Opt. Lett 23 (1998) 561, https://doi.org/10.1364/OL.23.000561.

[17] Hao Yang, Chaolong Song, Huabei Jiang, Novel Fluorescence Imaging Approach in Deep Tissue Based on Sonoluminescence, in: Biophotonics Congress: Biomedical Optics Congress 2018 (Microscopy/Translational/Brain/OTS), OSA, Washington, D.C., 2018: p. JW3A.16. https://doi.org/10.1364/TRANSLATIONAL.2018.JW3A.16.

[18] Y. Wang, Z. Yi, J. Guo, S. Liao, Z. Li, S. Xu, B. Yin, Y. Liu, Y. Feng, Q. Rong, X. Liu, G. Song, X.B. Zhang, W. Tan, In vivo ultrasound-induced luminescence molecular imaging, Nat. Photon. (2024) 334–343, https://doi.org/10.1038/s41566-024-01387-1.

[19] V. Vighetto, A. Troia, M. Laurenti, M. Carofiglio, N. Marcucci, G. Canavese, V. Cauda, Insight into Sonoluminescence Augmented by ZnO-Functionalized Nanoparticles, ACS Omega 7 (2022) 6591–6600, https://doi.org/10.1021/ACSOMEGA.1C05837.

[20] V. Vighetto, M. Conte, G. Rosso, M. Carofiglio, F. Sidoti Abate, L. Racca, G. Mesiano, V. Cauda, Anti-CD38 targeted nanotrojan horses stimulated by acoustic waves as therapeutic nanotools selectively against Burkitt's lymphoma cells, Discover, Nano 19 (2024) 1–20, https://doi.org/10.1186/S11671-024-03976-Z.

[21] M. Carofiglio, M. Conte, L. Racca, V. Cauda, Synergistic Phenomena between Iron-Doped ZnO Nanoparticles and Shock Waves Exploited against Pancreatic Cancer Cells, ACS. Appl. Nano. Mater 5 (2022) 17212–17225, https://doi.org/10.1021/acsanm.2c04211.

[22] L. Racca, T. Limongi, V. Vighetto, B. Dumontel, A. Ancona, M. Canta, G. Canavese, N. Garino, V. Cauda, Zinc oxide nanocrystals and high-energy shock waves: a new synergy for the treatment of cancer cells, Front. Bioeng. Biotechnol 8 (2020), https://doi.org/10.3389/FBIOE.2020.00577.

[23] B. Dumontel, F. Susa, T. Limongi, M. Canta, L. Racca, A. Chiodoni, N. Garino, G. Chiabotto, M.L. Centomo, Y. Pignochino, V. Cauda, ZnO nanocrystals shuttled by extracellular vesicles as effective Trojan nano-horses against cancer cells, Nanomedicine 14 (2019) 2815–2833, https://doi.org/10.2217/NNM-2019-0231.

[24] M. Carofiglio, M. Laurenti, V. Vighetto, L. Racca, S. Barui, N. Garino, R. Gerbaldo, F. Laviano, V. Cauda, Iron-Doped ZnO Nanoparticles as Multifunctional Nanoplatforms for Theranostics, Nanomaterials 2021, Vol. 11, Page 2628 11 (2021) 2628. https://doi.org/10.3390/NANO11102628.

[25] S. Barui, R. Gerbaldo, N. Garino, R. Brescia, F. Laviano, V. Cauda, Facile Chemical Synthesis of Doped ZnO Nanocrystals Exploiting Oleic Acid, Nanomaterials 2020, Vol. 10, Page 1150 10 (2020) 1150. https://doi.org/10.3390/NANO10061150.

[26] N. Garino, T. Limongi, B. Dumontel, M. Canta, L. Racca, M. Laurenti, M. Castellino, A. Casu, A. Falqui, V. Cauda, A Microwave-Assisted Synthesis of Zinc Oxide Nanocrystals Finely Tuned for Biological Applications, Nanomaterials 2019, Vol. 9, Page 212 9 (2019) 212. https://doi.org/10.3390/NANO9020212.

[27] B. Dumontel, M. Canta, H. Engelke, A. Chiodoni, L. Racca, A. Ancona, T. Limongi, G. Canavese, V. Cauda, Enhanced biostability and cellular uptake of zinc oxide nanocrystals shielded with a phospholipid bilayer, J. Mater. Chem. B 5 (2017) 8799–8813, https://doi.org/10.1039/C7TB02229H.

[28] M. Conte, M. Carofiglio, G. Rosso, V. Cauda, Lipidic Formulations Inspired by COVID Vaccines as Smart Coatings to Enhance Nanoparticle-Based Cancer Therapy, Nanomaterials 13 (2023) 2250, https://doi.org/10.3390/nano13152250.

[29] G. Rosso, G. Mesiano, B. Dumontel, M. Carofiglio, M. Conte, A. Grattoni, V. Cauda, Acoustic waves and smart biomimetic nanoparticles: combination treatment from 2D to 3D colorectal cancer models, Cancer. Nanotechnol 15 (2024) 1–23, https://doi.org/10.1186/S12645-024-00281-3.

[30] K.S. Hong, H. Xu, H. Konishi, X. Li, Direct water splitting through vibrating piezoelectric microfibers in water, J. Phys. Chem. Lett. 1 (2010) 997–1002, https://doi.org/10.1021/JZ100027T.

[31] C.P. Collier, T. Vossmeyer, J.R. Heath, Nanocrystal superlattices, Annu. Rev. Phys. Chem 49 (1998) 371–404, https://doi.org/10.1146/ANNUREV.PHYSCHEM.49.1.371.

[32] C. Pacholski, A. Kornowski, H. Weller, Self-assembly of ZnO: from nanodots to nanorods, Angew. Chem. Int. Ed. 41 (2002) 1188–1191, https://doi.org/10.1002/1521-3773(20020402)41:7<1188::AID-ANIE1188>3.0.CO;2-5.

[33] M. Canta, V. Cauda, The investigation of the parameters affecting the ZnO nanoparticle cytotoxicity behaviour: a tutorial review, Biomater. Sci 8 (2020) 6157–6174, https://doi.org/10.1039/D0BM01086C.

[34] B. Dumontel, F. Susa, T. Limongi, V. Vighetto, D. Debellis, M. Canta, V. Cauda, Nanotechnological engineering of extracellular vesicles for the development of actively targeted hybrid nanodevices, Cell Biosci. 2022 12:1 12 (2022) 1–18. https://doi.org/10.1186/S13578-022-00784-9.

[35] L. Racca, G. Rosso, M. Carofiglio, S. Fagoonee, G. Mesiano, F. Altruda, V. Cauda, Effective combination of biocompatible zinc oxide nanocrystals and high-energy shock waves for the treatment of colorectal cancer, Cancer. Nanotechnol 14 (2023) 1–21, https://doi.org/10.1186/S12645-023-00195-6.

[36] M. Carofiglio, G. Mesiano, G. Rosso, M. Conte, M. Zuccheri, Y. Pignochino, V. Cauda, Targeted lipid-coated ZnO nanoparticles coupled with ultrasound: A sonodynamic approach for the treatment of osteosarcoma as 3D spheroid models, Mater. Today. Commun 40 (2024) 109826, https://doi.org/10.1016/J.MTCOMM.2024.109826.